Atmos. Chem. Phys. Discuss., 15, 12491–12537, 2015
www.atmos-chem-phys-discuss.net/15/12491/2015/
doi:10.5194/acpd-15-12491-2015
© Author(s) 2015. CC Attribution 3.0 License.

Atmospheric Chemistry and Physics Discussions
Open Access

This discussion paper is/has been under review for the journal Atmospheric Chemistry and Physics (ACP). Please refer to the corresponding final paper in ACP if available.

Aerosol size distribution and new particle formation in western Yangtze River Delta of China: two-year measurement at the SORPES station

X. M. Qi[1,3], A. J. Ding[1,3], W. Nie[1,3], T. Petäjä[2], V.-M. Kerminen[2], E. Herrmann[1], Y. N. Xie[1], L. F. Zheng[1,3], H. Manninen[2], P. Aalto[2], J. N. Sun[1,3], Z. N. Xu[1,3], X. G. Chi[1,3], X. Huang[1,3], M. Boy[2,3], A. Virkkula[1,2,3], X.-Q. Yang[1,3], C. B. Fu[1,3], and M. Kulmala[2]

[1]Institute for Climate and Global Change Research & School of Atmospheric Sciences, Nanjing University, 210023, Nanjing, China
[2]Department of Physics, University of Helsinki, 00014 Helsinki, Finland
[3]Collaborative Innovation Center of Climate Change, Nanjing, Jiangsu Province, China

Received: 30 January 2015 – Accepted: 30 March 2015 – Published: 29 April 2015

Correspondence to: A. J. Ding (dingaj@nju.edu.cn)

Published by Copernicus Publications on behalf of the European Geosciences Union.

Abstract

Aerosol particles play important roles in regional air quality and global climate change. In this study, we analyzed two-year (2011–2013) of measurements of submicron particles (6–800 nm) at a suburban site in western Yangtze River delta (YRD) of East China. The number concentrations (NCs) of particles in the nucleation, Aitken and accumulation modes were 5300 ± 5500, 8000 ± 4400, $5800 \pm 3200\,\mathrm{cm}^{-3}$, respectively. Number concentrations and size distributions of submicron particles were also influenced by long-range and regional transport of air masses. The highest and lowest accumulation mode particle number concentrations were observed in air masses from YRD and coastal region, respectively. Continental air masses from inland had the highest concentrations of nucleation mode particles. New particle formation (NPF) events, apparent in 44 % of the effective measurement days, occurred frequently in all the seasons except winter. Radiation and pre-existing particles were found to be the main factors influencing the occurrence of NPF events. The particle formation rate was the highest in spring ($3.6 \pm 2.4\,\mathrm{cm}^{-3}\,\mathrm{s}^{-1}$), whereas the particle growth rate had the highest values in summer ($12.8 \pm 4.4\,\mathrm{nm\,h}^{-1}$). The formation rate was typically high in relatively clean air masses, whereas the growth rate tended to be high in the polluted YRD air masses. The frequency of NPF events and the growth rate showed a strong year-to-year difference. In the summer of 2013, associated with a multi-week heat wave and photochemical pollution, NPF events occurred more frequently and the growth rate was much higher than in the same period of 2012. The difference in the location and strength of sub-tropical High, which influences the air mass transport pathways and solar radiation, seems to be the driving cause for year-to-year differences. This study reported the longest continuous measurement records of submicron particles in the East China and gained a comprehensive understanding of the main factors controlling the seasonal and year-to-year variation of the aerosol size distribution and NPF in the East China. The work highlights the importance and need for long-term measurements in understanding the atmosphere system and the impact by human activities.

ACPD
15, 12491–12537, 2015

CC BY

1 Introduction

Atmospheric aerosols affect human life by influencing both air quality and climate (e.g. Charlson et al., 1992; Menon et al., 2002; Akimoto, 2003; Heal et al., 2012; IPCC, 2013). Fine particles, especially the submicron ones, have received lots of attention due to their close connection to climate via light extinction (Malm et al., 1994), cloud droplet activation (Kerminen et al., 2005; Wiedensohler et al., 2009; Sihto et al., 2011) and precipitation formation (Gettelman et al., 2013; Lebo and Feingold, 2014), as well as due to their adverse effects on human health (Pope et al., 2002; Rao et al., 2012)

In view of the above, numerous studies have been conducted all over the world focusing on the characters of submicron particles, including their chemical composition and size distribution as well as their formation and growth in the atmosphere (e.g. Woo et al., 2001; Birmili et al., 2003; Engler et al., 2007; Zhang et al., 2007; Dal Masoet al., 2008; Laakso et al., 2008; Jimenez et al., 2009; Komppula et al., 2009; Asmi et al., 2011; Kerminen et al., 2012; Vakkari et al., 2013; Kulmala et al., 2014; Nieminen et al., 2014). In China, studies on submicron particles started about a decade ago. However, to the best of our knowledge, there are only three studies in China providing more than one year of measurements of aerosol size distributions, with two of them conducted in North China Plain (Wu et al., 2007; Shen et al., 2011) and one at Mount Waliguan in remote western China (Kivekäs et al., 2009). Therefore, knowledge about the temporal variation of submicron particles and their relationship to the climatology and human activities in China is rather poor, even in some well-developed regions such as Yangtze River Delta (YRD) in East China.

The YRD has experienced rapid urbanization and industrialization in the last two decades, which have induced large amounts of fossil fuel consumption in the region and resulted in serious air pollution (Chameides et al., 2002; Ding et al., 2013a, b; Tie and Cao, 2009; Li et al., 2011). In addition, YRD is a region influenced by typical Asian monsoon, which dominates the temporal and spatial variations of particles (Qian et al., 2003; Ding et al., 2013a). However, previous studies on aerosols in this region were

ACPD
15, 12491–12537, 2015

CC BY

mainly on mass concentrations and chemical compositions (e.g. Huang et al., 2012; Cheng et al., 2013; Ding et al., 2013a), but studies on the number concentrations and size distributions were rather limited. In Nanjing, Herrmann et al. (2014) reported the first result of about 4-month data of aerosol size distribution at the SORPES station, a suburban site in Nanjing, and Wang et al. (2014) reported about one month data at another suburban site. Both studies were conducted during the cold season. In other regions of the YRD, Gao et al. (2009) reported an intensive campaign in the early summer of 2005 in Taicang, a small town nearby Shanghai, and Du et al. (2011) reported measurements from October 2008 to February 2009 in Shanghai. These results showed significant differences in both the diurnal patterns and NPF characters between the two seasons, and emphasize the need of continuous long-term measurements on the number size distributions of submicron particles in this region.

In the present study, we report two-year continuous observation of submicron particles (6–800 nm) and related quantities (including trace gases, $PM_{2.5}$ mass and meteorological data) recorded at the SORPES (Stations for Observing Regional Processes of the Earth System) site in suburban Nanjing of western YRD from December 2011 to November 2013. The aim of this work is to characterize the temporal variations of particle number size distributions and occurrence of new particle formation (NPF) in the western part of YRD, and to improve our understanding on the sources and processes influencing the atmospheric aerosol population in the developed region in China.

2 Experiment and methodology

2.1 Site information and measurements

This study was conducted at the SORPES station developed in 2011 (Ding et al., 2013a). The site is located about 20 km northeast of downtown Nanjing (118°57′10″ E, 32°07′14″ N, 40 m a.g.l.). With few local sources within 2–3 km surround, it can be considered as a regional background site in the well-developed YRD of East China. More

ACPD
15, 12491–12537, 2015

CC BY

details of the site, including trace gas, $PM_{2.5}$ and meteorological measurements, can be found in Ding et al. (2013a).

Size distribution of submicron particles is measured with a DMPS (Differential Mobility Particle Sizer) constructed at the University of Helsinki in Finland. This instrument was also involved in the instrument inter-comparison workshops conducted within the European infrastructure project EUSAAR (European Supersites for Atmospheric Aerosol Research) and ACTRIS (Aerosols, Clouds, and Trace gases Research Infrastructure Network) (Wiedensohler et al., 2012). Before entering the inlet of the instrument, the particles are cut off at 2.5 µm and then dried (using Nafion tube from December 2011 to June 2012 and silica gel dryer after June 2012). The instrument consists of one DMA (Differential Mobility Analyzer) in different flow rates and one CPC (Condensation Particle Counter, TSI Model 3772). The DMA segregates the particles into exact narrow size ranges based on different, narrow ranges of electrical mobilities of charged particles in the electrical field. Equilibrium charge is ensured by two Americium 241 sources (each about 37 kBq) before particles enter the DMA. The DMPS is a flow-switching type differential mobility particle sizer in which two different sample and sheath air flow rates for the DMA are used to cover a wide size range. In the high flow mode, the sample air and sheath air flows are 3 and 20 $L\,min^{-1}$, respectively, and in the low flow mode they are 1 and 5 $L\,min^{-1}$, respectively. The high flow mode measures the size from 6 to 100 nm and the low flow mode measures from 100 to 800 nm. The measurement time interval of the instrument is 10 min during which the total particle number concentration are measured by CPC directly and 29 channels (16 for low flow rate and 13 for high flow rate) are scanned. Weekly maintenance, including flow rate adjusting and impactor cleaning, is routinely performed. About the data assimilation in two flow modes and the test of data quality are described in Appendix.

2.2 Calculation of variables characterizing new particle formation

The calculation of particle growth and formation rates along with the condensation sink was made following the procedure described by Kulmala et al. (2012). The growth rate

ACPD
15, 12491–12537, 2015

CC BY

(GR) of particles during the NPF events can be expressed as:

$$\mathrm{GR} = \frac{\mathrm{d}d_\mathrm{p}}{\mathrm{d}t} = \frac{\Delta d_\mathrm{p}}{\Delta t} = \frac{d_{\mathrm{p}2} - d_{\mathrm{p}1}}{t_2 - t_1} \tag{1}$$

where $d_{\mathrm{p}1}$ and $d_{\mathrm{p}2}$ are the representative of the diameter of nucleated particles at the times t_1 and t_2, respectively. For calculation, $d_{\mathrm{p}1}$ and $d_{\mathrm{p}2}$ are defined as the centre of size bin and t_1 and t_2 are the times when the concentration of this size bin reaches the maximum.

The formation rate of particles of diameter d_p is obtained from:

$$J_{d_\mathrm{p}} = \frac{\mathrm{d}N_{d_\mathrm{p}}}{\mathrm{d}t} + \mathrm{CoagS}_{d_\mathrm{p}} \times N_{d_\mathrm{p}} + \frac{\mathrm{GR}}{\Delta d_\mathrm{p}} \times N_{d_\mathrm{p}} + S_\mathrm{losses} \tag{2}$$

where the first term on the right side is the time evolution of the particle number concentration in the size range $[d_\mathrm{p}, d_\mathrm{p} + \Delta d_\mathrm{p}]$. The second term is the coagulation loss approximated by the product of coagulation sink ($\mathrm{CoagS}_{d_\mathrm{p}}$) and the number concentration in the size range $[d_\mathrm{p}, d_\mathrm{p} + \Delta d_\mathrm{p}]$. The third term is the growth out of the considered size range where GR is the observed growth rate. The fourth term represents additional losses which were not considered in this study.

Having positive correlation with coagulation sink (CoagS), condensation sink (CS) describes the speed at which condensable vapour molecules condense onto the existing aerosol. It is expressed as:

$$\mathrm{CS} = 4\pi \int_0^{d_\mathrm{p}\mathrm{max}} \beta_\mathrm{m}\left(d'_\mathrm{p}\right) d'_\mathrm{p} N_{d'_\mathrm{p}} \mathrm{d}d'_\mathrm{p} = 4\pi D \sum_{d'_\mathrm{p}} \beta_{\mathrm{m},d'_\mathrm{p}} d'_\mathrm{p} N_{d'_\mathrm{p}} \tag{3}$$

where D is the diffusion coefficient of the condensing vapour, β_m is a transition-regime correction, d'_p is the discrete diameter and $N_{d'_\mathrm{p}}$ is the particle number concentration in respective size bin.

ACPD
15, 12491–12537, 2015

CC BY

3 Results and discussions

3.1 Particle number concentrations and size distributions

3.1.1 Overall results

Figure 1a shows the averaged particle number size distribution during the studied period. It shows a typical multimodal distribution as a result of combination of three log-normal distributions in the nucleation (6–30 nm), Aitken (30–100 nm) and accumulation modes (100–800 nm). Figure 1b illustrates the average fraction of the particle number, surface and volume concentration in these three modes. It shows features similar to most other continental regions in the lower troposphere, i.e. the nucleation and Aitken mode particles (< 100 nm) dominate the number concentration, and accumulation mode particles control the surface and volume concentration (Raes et al., 2000; Asmi et al., 2011).

As shown in Table 1, the average (± SD) total particle number concentration (NC) over the diameter range 6–800 nm during the two-year period was 19 200 ± 9200 cm^{-3}, with the values of 5300 ± 5500 cm^{-3} in the nucleation mode (6–30 nm), 8000 ± 4400 cm^{-3} in the Aitken mode (30–100 nm) and 5800 ± 3200 cm^{-3} in the accumulation mode (100–800 nm), respectively. Compared with the other three reported long-term studies in China, the total particle NC measured at SORPES in Nanjing are comparable to those measured at the urban site in Beijing (about 32 700 cm^{-3} in the size range of 3–1000 nm) (Wu et al., 2008), higher than those measured at a rural site near Beijing (about 11 500 cm^{-3} in the size range of 3–1000 nm) (Shen et al., 2011), and about 10 times higher than those measured at Mount Waliguan, a background site in a remote region of western China (about 2100 cm^{-3} in the size range of 12–570 nm) (Kivekäs et al., 2009). One typical feature of submicron particles at SORPES is the very high concentration of accumulation mode particles, being several times higher than typical concentrations measured in Europe or North America (200 to 2900 cm^{-3}

ACPD
15, 12491–12537, 2015

CC BY

compared to 5700 cm^{-3} at SORPES in the size range of 100–500 nm) (Stanier et al., 2004; Asmi et al., 2011; Wang et al., 2011).

3.1.2 Seasonal variations

The average seasonal variations of the total particle number concentration and number concentrations in the three modes are presented in Fig. 2. During the two-year measurement period, nucleation mode particles had elevated concentrations in early winter and spring. Aitken mode particles show a similar pattern, except that they had a weaker month-to-month variability than nucleation mode particles and peak in summer. Compared with the other two modes, accumulation mode particles showed a weaker seasonal variation with a peak in January and lowest concentrations in July. As accounting for almost 70 % of the total particles, the nucleation and Aitken mode particles dominated the seasonal cycle of the total particle number concentration. The exact values and SDs of the particle number concentrations in different seasons are given in Table 1. Seasonally, the nucleation and Aitken mode particles showed the highest concentrations in spring ($6200 \pm 5900\ cm^{-3}$ and $8500 \pm 4000\ cm^{-3}$, respectively), whereas highest concentration of accumulation mode particles were observed in winter ($6500 \pm 3000\ cm^{-3}$). The geometric mean diameter (GMD) of the particles and condensation sink (CS) revealed also seasonal variation (Table 1), with the highest values observed in winter (97 ± 26 nm, $4.8 \times 10^{-2} \pm 2.3 \times 10^{-2}\ s^{-1}$).

Generally, the seasonal patterns of NC of submicron particles at SORPES were related to the long-range transport associated with the Asian monsoon climate and also anthropogenic emissions. Figure 3 presents the seasonal variations of four meteorological variables (temperature, pressure, radiation and rainfall) during the two-year measurement period. In winter, few rains and lower boundary layer favor the accumulation of pollutants and result in high particle loadings. In summer, the dominantly rainy and unstable weather (e.g. convection and monsoon precipitation) leads to low particle number concentrations, especially for accumulation mode particles. Radiation

ACPD
15, 12491–12537, 2015

CC BY

connected with NPF events and local direct emissions from vehicles influenced the NC of nucleation and Aitken mode particles. In addition, an evident holiday effect can also influence the observed temporal variation. For example, the low particle loadings in all the modes can be identified in February (see Fig. 2) when Chinese have the winter break to celebrate the Spring Festival (Ding et al., 2013a).

Biomass burnings (BB) is an important source of accumulation mode particles in early summer (Ding et al., 2013a, b), so the burning of wheat straw in northern and middle part of East China (Wu et al., 2008; Shen et al., 2010) is the plausible cause for the observed particle NCs peak in June (Fig. 2d). The average NC of accumulation mode particles during BB events in June (BB event is defined as potassium concentration $K^+ > 2\,\mu g\,cm^{-3}$ and $K^+/PM_{2.5}$ ratio > 0.02 at SORPES, K^+ was measured using MARGA) is $31\,700\,cm^{-3}$, that is almost 5 times higher than the corresponding NC in non-BB event days ($5300\,cm^{-3}$). Relatively large (> 100 nm) particles are emitted directly from BB (Reid et al., 2005; Li et al., 2007), or formed rapidly after emissions by the combination of NPF and various particle growth processes (Hennigan et al., 2012; Vakkari et al., 2014). Such particles are able to promote atmospheric heterogeneous chemistry by providing a large surface area (Nie et al., 2014), influence the global climate by enhancing the CCN capacity (Hennigan et al., 2012), and even change the everyday weather (Ding et al., 2013b).

3.1.3 Diurnal pattern in different seasons

The diurnal cycles of particle number size distributions had similar patterns in spring, summer and autumn, which were connected to the events of new particle formation and growth, showing the typical "banana" shape during daytime (Fig. 4a–c). However, obvious differences could be observed for the starting time and strength of NPF in different seasons. A detailed discussion on NPF events will be given in Sect. 3.2. In winter, direct emissions from vehicles might play a key role in the diurnal cycle of particle number size distributions, such as the peak concentrations in all of the three modes during the rush hours in the morning and late afternoon (Fig. 4d).

ACPD
15, 12491–12537, 2015

CC BY

In order to investigate the detailed diurnal variations of the particle NCs in different modes, we selected typical seasons of spring and winter to compare their diurnal patterns in the three modes (Fig. 5a–c). For nucleation mode particles, peak concentrations appeared at noontime in spring but at the early morning or later afternoon in winter. The later suggests a possible influence from human activities, such as vehicle emissions under conditions of a low mixing layer. For the Aitken mode particles, in spring the highest concentrations were seen about two hours after the appearance of the peak in the nucleation mode, which was due to the growth of nucleated particles to larger sizes (Fig. 5b). In winter, Aitken mode particles had peaks at the same time or a bit later than what the nucleation mode particle did. The diurnal variation of the accumulation mode particle number concentration (Fig. 5c) was controlled by the development of the boundary layer in both seasons, having a pattern similar to that of the $PM_{2.5}$ concentration (Ding et al., 2013a).

3.1.4 The influences of air masses

Figure 6 shows backward trajectory cluster analysis for the SORPES site. Using the Hybrid Single-Particle Lagrangian Integrated Trajectory (HYSPLIT) model Version 4.9 (Draxler and Hess, 1998) driven with Global Data Assimilation System (GDAS) output, 5 clusters of trajectories were identified based on hourly 2-day backward trajectories for the period of December 2011–November 2013. The results show that air masses arriving at the SORPES site generally came from the inland continent (C2 and C3, 14.8 and 13.0 %, respectively), coastal North China (C1, 30.6 %) or Yangtze River Delta (C4 and C5, 41.6 % in total). The air mass transport pattern was controlled by Asian monsoon (Ding et al., 2013a), with winter monsoon bringing regional pollution from the North China Plain (C2, C1 and C5) and summer monsoon bringing the YRD regional pollution (C4) or biogenic emissions from the South China to the site (C3). Being located in the most western part of the YRD, SORPES is a unique site to investigate the impact of different regional air masses.

ACPD
15, 12491–12537, 2015

CC BY

The statistics of the particles number size distributions and diurnal variations of NC in the three modes for the three different air masses (Coastal (C1), Continental (C2 and C3) and YRD (C4 and C5) air masses) are shown in Fig. 7. The coastal air mass had the lowest accumulation mode particle loading during the whole day (Fig. 7d). With low pre-existing particle loading and favorable meteorological conditions, e.g. sunny days with high radiation, NPF events easily occur and cause high amounts of nucleation and Aitken mode particles during the daytime (Fig. 7b and c). The continental air mass had highest levels of nucleation mode particles (Fig. 7b) because such air masses are always associated with sunny days and low humidity. In addition, since the site is located in the northeast of downtown Nanjing, continental C3 air masses generally bring fresh, directly-emitted particles, i.e. Aitken mode particles, to the site. The YRD air masses, passing through the YRD city clusters, always led to the highest accumulation mode particles loadings (Fig. 7d), lowering concentrations of nucleation mode particles (Fig. 7b) via higher coagulation/condensation sinks.

3.2 New particle formation (NPF)

3.2.1 Population statistic about NPF

During the 2-year measurement period, the sampling days were classified into NPF event days, non-event days and no-data/undefined days with the criterion whether a burst occurred for the nucleation mode particles. By following the method used by Dal Maso et. al. (2005) and Kulmala et al. (2012), the event days were further classified into Class I when the formation and growth rate can be calculated with confidence, and Class II when the formation and growth rate cannot be calculated or done in accurate ways.

The numbers of the four types of sampling days are given in Table 2, and the percentage of event days (the ratio of Class I days or Class II days to event days and non-event days) in each month are shown in Fig. 8a. Due to instrument maintenance, data from 111 days of the two-year period were unavailable for the event classification. Only few

ACPD
15, 12491–12537, 2015

CC BY

of the days at SORPES were considered as undefined days (11 days), for which it was hard to determine whether a NPF event occurred or not. Overall, NPF event days (including Class I and Class II days) accounted for 44 % of the analyzed days (sample days excluded no-data/undefined days). This frequency is a bit higher than observed in the other two long-term measurements in China (urban Beijing ~ 40 %, SDZ ~ 37 %). In spring, summer and autumn, NPF events took place in more than 50 % of analyzed days (56, 55 and 50 %, respectively), which is more frequent than at other measurement sites in China, including as Taicang (44 %), Hong Kong (34 %) and Xinken (26 %) (Gao et al., 2008; Guo et al., 2012; Liu et al., 2008). In contrast, in winter only 15 NPF event days during two-year measurement period were identified. This frequency is similar to another work in Shanghai (Du et al., 2012), but quite different from that in Beijing where winter is the second season favorable to NPF (Wu et al., 2007; Shen et al., 2011). One explanation for this could be that there are more "clean" days in winter in Beijing because of frequent cold fronts (Wehner et al., 2008). Such fronts were generally not strong enough to improve the air quality in Nanjing. In June, continuous rainy days ("Plum rain" in China) with low radiation also inhibit the NPF events. There was a great difference in the frequency of NPF events in summer between the two years: 41 % in 2012 and 66 % in 2013 (Fig. 8a).

Figure 8b gives the variability of start and end times of the Class I event days. Since the cut-off diameter of the DMPS was 6 nm, the start and end times were defined here as the times when the 6–7 nm particles started to increase and decrease back to the background level (i.e. ~ 50 cm^{-3}). Generally, the start time was somewhere between the sunrise and midday, and no evident nocturnal events were identified. The seasonal variation of the start time followed that of sunrise, which is similar to reported elsewhere around the world (e.g. Woo et al., 2001; Boy and Kulmala, 2002; Kulmala et al., 2004; Hamed et al., 2007; Wu et al., 2007). However, at some days the start time was just one hour after the sunrise. Most of such events took place in summer and were associated with marine air masses that had been transported over the polluted area in YRD. This topic will be studied further in our future work.

ACPD
15, 12491–12537, 2015

CC BY

The formation rate of 6 nm particles (J_6) and growth rate of 6 to 30 nm particles ($GR_{6–30\,nm}$) during the Class I event days are illustrated in Fig. 8c and d. The statistical results are given in Table 2. The formation rates were highest in spring with the value of $3.6 \pm 2.4\,cm^{-3}\,s^{-1}$, followed by summer ($2.1 \pm 1.4\,cm^{-3}\,s^{-1}$) and autumn ($2.1 \pm 1.9\,cm^{-3}\,s^{-1}$), whereas the lowest formation rates were observed in winter ($1.8 \pm 1.6\,cm^{-3}\,s^{-1}$). The maximum formation rate was $10.9\,cm^{-3}\,s^{-1}$ on 3 April 2013. The observed formation rates are comparable to other measurements in China, e.g. 3.3–$81.4\,cm^{-3}\,s^{-1}$ in Beijing, 0.7–$72.7\,cm^{-3}\,s^{-1}$ at SDZ and 2.2–$19.8\,cm^{-3}\,s^{-1}$ (3 October–5 November 2004) in PRD (for J_3), 0.97–$10.2\,cm^{-3}\,s^{-1}$ (25 October–29 November 2010) in Hong Kong (for $J_{5.5}$), and 1.2–$2.5\,cm^{-3}\,s^{-1}$ (5 May–2 June 2005) in Shanghai (for J_{10}) (Wu et al., 2007; Shen et al., 2011; Liu et al., 2008; Guo et al., 2012; Gao et al., 2008). Concerning the nuclei growth rates, the highest values of $12.8 \pm 4.4\,nm\,h^{-1}$ were observed in summer, followed by spring ($10.0 \pm 3.4\,nm\,h^{-1}$), winter ($9.5 \pm 3.3\,nm\,h^{-1}$) and autumn ($8.9 \pm 2.9\,nm\,h^{-1}$). The maximum growth rate was $22.9\,nm\,h^{-1}$, observed on 29 August 2013. The values of growth rates presented in this study for Nanjing are slightly higher than reported for the other two long-term measurements in China, i.e. 0.1–$11.2\,nm\,h^{-1}$ in Beijing and 0.3–$14.5\,nm\,h^{-1}$ with mean value of $4.3\,nm\,h^{-1}$ at SDZ (Wu et al., 2007; Shen et al., 2011). Condensation sink that tends to limit to NPF, was generally lower on event days compared with non-event days ($3.1 \times 10^{-2}\,s^{-1}$ for Class I, $3.6 \times 10^{-2}\,s^{-1}$ for Class II, and $4.2 \times 10^{-2}\,s^{-1}$ for non-event days).

3.2.2 Conditions favoring NPF

In Fig. 9, we compare the quantities that may affect NPF between the event (Class I and Class II) and non-event days in different seasons. Precursors, solar radiation and pre-existing particles have been generally considered as the major factors influencing the NPF (McMurry et al., 2005; Kulmala and Kerminen, 2008; Kulmala et al., 2013). As shown in Fig. 9a and d, radiation and O_3 concentration were significantly higher on event days than those on non-event days, indicating that the observed NPF events in

ACPD
15, 12491–12537, 2015

CC BY

YRD were typically photochemical influenced. Higher temperatures and lower RH favored the occurrence of NPF events. A higher temperature may enhance the reaction rates of the chemical processes producing nucleating vapors, and a lower RH may decrease the sink of these vapors as well as the sink of newly-formed molecular clusters. The relation between NPF and $PM_{2.5}$ was quite clear in all the seasons, with lower $PM_{2.5}$ concentrations favoring the occurrence of NPF events (Fig. 9e).

The role of SO_2 seemed to be a complex issue in YRD. Generally, high concentrations of SO_2, being the precursor for gaseous sulfuric acid, should promote the occurrence of NPF. In this study, SO_2 concentrations were higher in event days than in non-event days in both spring and summer, whereas the opposite was seen in autumn and winter. This result was in accordance with our previous study conducted in winter time that suggested NPF to occur preferably under conditions of lower SO_2 concentrations (Herrmann et al., 2014). In polluted regions of China, like YRD, SO_2 concentrations are generally at a high level with average concentrations of about 10 ppb, which is sufficient and seems not to be a limiting factor for NPF. Instead, the pre-existing particles, e.g. $PM_{2.5}$, play a more important role as coagulation and condensation sink. Given that the SO_2 peaks were always accompanied with a high $PM_{2.5}$ concentration in this region, especially in autumn and winter, the observed lower SO_2 concentrations in event days in autumn and winter are therefore understandable.

3.2.3 Factors influencing formation rate and growth rate

To investigate the factors that influence the formation rate and growth rate, the correlation coefficients of J_6, $GR_{6–30\,nm}$ and CS with meteorological quantities and gaseous pollutants were calculated (Table 3). The correlation coefficients that passed the statistical significance test ($p < 0.05$) were highlighted by asterisk in Table 3. The particle formation rate (J_6) was negatively correlated with RH and positively correlated with both radiation and O_3. No correlation between J_6 and SO_2 was seen, which supports the view that SO_2 concentrations are not limiting NPF in YRD. The particle growth rate was positively correlated with temperature, RH, radiation, O_3 and CS ($p < 0.05$).

ACPD
15, 12491–12537, 2015

CC BY

Worth noting here is that while lower values of RH and CS appeared to favor the occurrence of a NPF event, higher values of these two quantities clearly favored the particle growth. The scatter plots of J_6–RH and $GR_{6–30\,nm}$–RH color-coded with O_3 mixing ratio are shown in Fig. 10. The negative correlation between J_6 and RH did not depend on the O_3 concentration (Fig. 10a), whereas for $GR_{6–30\,nm}$ an obvious difference in the $GR_{6–30\,nm}$–RH slope could be identified for different levels of the O_3 mixing ratio (Fig. 10b). A higher slope for high-O_3 events suggests a link between the particle growth and photochemical pollutants.

In order to study further the event with high or low value of $J_6/GR_{6–30\,nm}$, we conducted Lagrangian dispersion modeling for the selected days marked in Fig. 8c and d, by using the method developed by Ding et al. (2013c) based on HYSPLIT model to study the influence of air masses. Figure 11 gives the footprint, i.e. retroplume at an altitude of 100 m, of the selected high and low $J_6/GR_{6–30\,nm}$ days. Air masses had an obvious influence on the formation rate and growth rate. Most low J_6 days and high GR days occurred in the air masses passing over the polluted YRD area, while all the high J_6 days and low GR days appeared in air masses that did not go through the YRD area. This confirms that the polluted YRD plume may inhibit the formation of new particles, yet simultaneously promote the particle growth. In winter when solar radiation is low, no NPF events occurred in the YRD area masses that tend to have high pre-existing particle loadings (Herrmann et al., 2014). Our finding that the polluted YRD plume induces a high GR is consistent with the studies reporting relatively high particle growth rates under urban conditions (Kulmala and Kerminen, 2008; Peng et al., 2014).

3.3 Causes on the high frequency of NPF in August 2013

As shown in Fig. 8, a higher frequency of NPF events occurred in July and August of 2013 compared with the same months in 2012. In August of 2013, the frequency of Class I NPF events was highest during the two-year measurement period, with 17 Class I events observed among the 24 analyzed days. Figure 12 shows the time series of particle number size distribution, O_3 and $PM_{2.5}$ concentrations and radiation.

ACPD
15, 12491–12537, 2015

CC BY

The daily-average O_3 concentration gradually increased in early August with an hourly maximum value up to 165 ppbv on 12 August 2013. Accompanied with this O_3 episode, the geometric mean diameter (GMD) of submicron particles and $PM_{2.5}$ concentration also increased (Fig. 12a and b). Interestingly, there were continuously multi-day NPF events in the first half of this month, even during 11–13 August when $PM_{2.5}$ reached 70–80 $\mu g\,m^{-3}$. During 17–24 August, there were also notable NPF events. Contrary to this, few NPF took place in August 2012.

Examination of average geopotential height and wind vector at the 925 hPa level during the two Augusts (Fig. 13a) suggests that in 2013 the subtropical (Pacific) High moved more to the west than that in 2012, causing a positive anomaly (high pressure) and anti-cyclone over the Southeast China (Fig. 13b). As a result, the Yangtze River Delta experienced a continuous heat wave with humid and hot air transported from the south and southwest.

In order to further understand the air masses history during the events in 2013, Fig. 14 gives the averaged "footprint" (i.e., 100 m retroplume) for the episode period. The air masses can be divided into three time periods. During 6–11 August, the air masses came from the southwest with high value of BVOCs and they also passed through the downtown of Nanjing. During this period, O_3 was produced and accumulated with enough precursors and strong solar radiation. High O_3 concentrations also caused a strong atmospheric oxidation capacity, which caused an increase in the GMD of submicron particles together with an increase in the $PM_{2.5}$ mass concentration. On 11 August, the air masses transport pathway was changed, with air masses coming mainly from southeast and the YRD city cluster, which is the most polluted area with high value of anthropogenic VOCs and other pollution gases. Therefore, the O_3 concentration continued to increase until 12 August and then maintained a high level until 19 August. A common character of the air masses during both of these two periods was that the air had transported over regions with high biogenic and anthropogenic emissions (see Figs. 6a, b and 14). During 19 to 22 August, the air masses were mainly from northeast and had a high humidity that caused cloudy days with low radiation

ACPD
15, 12491–12537, 2015

CC BY

and high wet deposition. The O_3 concentration, GMD of submicron particles and $PM_{2.5}$ mass concentration therefore sharply decreased on 19 August.

Despite the high levels of GMD, $PM_{2.5}$ and CS (which is not shown in Fig. 12), Class I NPF events occurred every day during the whole O_3 episode (from 4 to 19 August 2013). As the GMD and $PM_{2.5}$ increased, the particle formation rates became lower. This means that the high values of GMD and $PM_{2.5}$ suppressed new particle formation but could not stop the occurrence of NPF event altogether under such an atmospheric condition of a high oxidization capacity. Because of lower pre-existing particle loading after 19 August, new particle formation continued although the radiation intensity and atmospheric ozone oxidation capacity were lower. Another obvious character for the August 2013 was that, during the whole month, the particle growth rate had a relatively high correlation with RH (with $r = 0.54$), supporting the positive correlation between GR and RH illustrated above (Fig. 15).

Here the year-to-year difference in aerosol size distributions and NPF characteristics suggests that large-scale circulations together with meteorological factors had a strong impact on the aerosol number concentration. Extreme meteorological conditions are able to reshape the seasonal profile of the aerosol number concentration and NPF, which means that measurements in a specific year cannot gain a full picture of seasonal profiles. Given the fact that there are only a limited number of measurements covering more than one year, especially in China, this work highlights the importance of long-term continuous measurement.

4 Summary

This study reports a two-year measurement (from December 2011 to November 2013) period of submicron particles (6–800 nm) at the SORPES station located in suburban Nanjing in the western part of YRD, East China, with the aim to characterize the temporal variation of the particle number concentration and size distribution, and to understand the new particle formation occurring in such a polluted monsoon area.

ACPD
15, 12491–12537, 2015

CC BY

The average total number concentrations was 19 200 ± 9200 (mean ± SD) cm^{-3}, with 5300 ± 5500 cm^{-3} in the nucleation mode (6–30 nm), 8000 ± 4400 cm^{-3} in the Aitken mode (30–100 nm) and 5800 ± 3200 cm^{-3} in the accumulation mode (100–800 nm). Seasonal variations of NC and size distribution were influenced by the Asian monsoon, anthropogenic activities and atmospheric oxidation capacity. The diurnal pattern of the particle number size distribution in winter showed peaks at the normal rush hours, suggesting the source from direct emissions of vehicles. Air mass long-range transportation played clear roles in influencing the particle number concentration: coastal air masses had lowest concentrations of accumulation mode particles but relatively high concentrations of nucleation mode particles, continental air masses had the highest concentrations of nucleation mode particles with frequent new particle formation, and YRD air masses had the highest concentrations of accumulation mode particles and lowest concentration of nucleation mode particles because of the elevated coagulation/condensation sinks.

NPF events were observed on 44 % of the analyzed days, with the highest frequency in spring, followed by summer and autumn, but only 15 event days in winter. The average formation rates of 6 nm particles were 3.6 ± 2.4, 2.1 ± 1.4, 2.1 ± 1.9 and 1.8 ± 1.6 $cm^{-3}\,s^{-1}$ in spring, summer, autumn and winter, respectively, and the corresponding particle growth rates were 10.0±3.4, 12.8±4.4, 8.9±2.9 and 9.5±3.3 $nm\,h^{-1}$. The intensity of radiation and loading of pre-existing particles seemed to be the main factors influencing the NPF events. SO_2 concentrations in YRD were always sufficient and appeared not to limit NPF. The particle formation rate was negatively correlated with RH and positively correlated with radiation and O_3 while particle growth rate was positively correlated with temperature, RH, radiation, O_3 and CS. Both particle formation and growth rate depended on the air mass origin, with low J_6 and high GR typical for polluted YRD air masses and high J_6 and low GR for clean air masses.

The observed frequency of NPF events and particle growth rate in summer showed a strong year-to-year variation under the influence of different large-scale circulations, such as subtropical High. Long-range transport, meteorological parameters and photo-

ACPD
15, 12491–12537, 2015

CC BY

chemical pollutants promoted the atmospheric new particle formation and growth in the summer 2013 compared with the previous year. To quantitatively understand the processes controlling the aerosol number concentration and size distribution, or to predict their behavior, additional modeling work on NPF that relies on long-term observations should be conducted in the future.

Appendix: Performance of the flow-switching DMPS

The flow-switching DMPS has two flow modes to measure the particles in two size ranges, 6–100 and 100–800 nm, respectively. To assimilate data in the two flow modes, in this study the number concentrations of particles in the size range from 100 to 800 nm were multiplied by a factor to make the particle number size distribution smooth. The correction was done for daily data. The average correction factor was 1.05 ± 0.11, which means that in this size range the original inverted number concentrations increased on the average by 5 %. The 10th, 25th, 50th, 75th and 90th percentiles of this correction factor were 0.92, 0.96, 1, 1.1 and 1.2, respectively.

The model of CPC used in this study was the TSI 3772 with the 10 nm default cut-off diameter when the condenser temperature is at the default value of 22 °C. It was set to 10 °C in this measurement, so the temperature difference ΔT between the saturator and the condenser was higher ($\Delta T > 25$ °C) which leads to a higher supersaturation and a lower cut-off diameter. The counting efficiency of 6 nm particles is higher than 75 % (Wiedensohler et al., 2012).

The DMPS was set up so that every time before number size distribution measurement, the DMA was by-passed, and total aerosol number concentration was determined directly by the CPC (Yli-Juuti et al., 2009). The average ratio of the total particle number concentration of that integrated from the inverted size distributions and measured directly with the CPC (N_{DMPS} and N_{CPC}) was 0.90 ± 0.17 and the correlation coefficient was 0.91 ($p < 1 \times 10^{-6}$). The 10th, 25th, 50th, 75th and 90th percentiles

ACPD
15, 12491–12537, 2015

CC BY

were 0.71, 0.82, 0.91, 0.99 and 1.06, respectively. These values can indicate that data quality of the DMPS was satisfactory.

Figure A1 shows the scatter plot of N_{DMPS} and N_{CPC} color-coded with the geometric mean diameter of the whole particle number size distribution ($GMD_{6–800\,nm}$). The ratio of N_{DMPS} to N_{CPC} was low when the $GMD_{6–800\,nm}$ was small but close to 1 when the $GMD_{6–800\,nm}$ was large. As the small $GMD_{6–800\,nm}$ corresponds to new particle formation events with a high concentration of nucleation mode particles, the lower N_{DMPS}-to-N_{CPC} ratio suggests that the DMPS (including the inversion) may have underestimated the concentration of them. This is in line with the inter-comparison study presented by Wiedensohler et al. (2012) where it was found that the largest uncertainties of the size distributions were in the nucleation mode.

Acknowledgements. This work was supported by the National Natural Science Foundation of China (D0512/41305123 and D03/41321062). The SORPES-NJU stations were supported by the '985 Program. Part of this work was supported by the Jiangsu Provincial Science Fund for Distinguished Young Scholars awarded to A. J. Ding (No. BK20140021) and by the Academy of Finland projects (1118615, 139656) and the European Commission via ERC Advanced Grant ATM-NUCLE.

References

Akimoto, H.: Global air quality and pollution, Science, 302, 1716–1719, doi:10.1126/science.1092666, 2003.

Asmi, A., Wiedensohler, A., Laj, P., Fjaeraa, A.-M., Sellegri, K., Birmili, W., Weingartner, E., Baltensperger, U., Zdimal, V., Zikova, N., Putaud, J.-P., Marinoni, A., Tunved, P., Hansson, H.-C., Fiebig, M., Kivekäs, N., Lihavainen, H., Asmi, E., Ulevicius, V., Aalto, P. P., Swietlicki, E., Kristensson, A., Mihalopoulos, N., Kalivitis, N., Kalapov, I., Kiss, G., de Leeuw, G., Henzing, B., Harrison, R. M., Beddows, D., O'Dowd, C., Jennings, S. G., Flentje, H., Weinhold, K., Meinhardt, F., Ries, L., and Kulmala, M.: Number size distributions and seasonality of submicron particles in Europe 2008–2009, Atmos. Chem. Phys., 11, 5505–5538, doi:10.5194/acp-11-5505-2011, 2011.

Birmili, W., Berresheim, H., Plass-Dülmer, C., Elste, T., Gilge, S., Wiedensohler, A., and Uhrner, U.: The Hohenpeissenberg aerosol formation experiment (HAFEX): a long-term study including size-resolved aerosol, H_2SO_4, OH, and monoterpenes measurements, Atmos. Chem. Phys., 3, 361–376, doi:10.5194/acp-3-361-2003, 2003.

Boy, M. and Kulmala, M.: Nucleation events in the continental boundary layer: Influence of physical and meteorological parameters, Atmos. Chem. Phys., 2, 1–16, doi:10.5194/acp-2-1-2002, 2002.

Chameides, W. L., Luo, C., Saylor, R., Streets, D., Huang, Y., Bergin, M., and Giorgi, F.: Correlation between model-calculated anthropogenic aerosols and satellite-derived cloud optical depths: indication of indirect effect?, J. Geophys. Res., 107, 4085, doi:10.1029/2000JD000208, 2002.

Charlson, R. J., Schwartz, S. E., Hales, J. M., Cess, R. D., Coakley Jr., J. A., Hansen, J. E., and Hofmann, D. J.: Climate forcing by anthropogenic aerosols, Science, 255, 423–430, doi:10.1126/science.255.5043.423, 1992.

Cheng, Z., Wang, S. X., Jiang, J. K., Fu, Q. Y., Chen, C. H., Xu, B. Y., Yu, J. Q., Fu, X., and Hao, J. M.: Long-term trend of haze pollution and impact of particulate matter in the Yangtze River Delta, China, Environ. Pollut., 182, 101–110, doi:10.1016/j.envpol.2013.06.043, 2013.

Dal Maso, M., Kulmala, M., Riipinen, I., Wagner, R., Hussein, T., Aalto, P. P., and Lehtinen, K. E. J.: Formation and growth of fresh atmospheric aerosols: eight years of aerosol size distribution data from SMEAR II, Hyytiälä, Finland, Boreal Environ. Res., 10, 323–336, 2005.

Dal Maso, M., Hyvärinen, A., Komppula, M., Tunved, P., Kerminen, V.-M., Lihavainen, H., Viisanen, Y., Hansson, H.-C., and Kulmala, M.: Annual and interannual variation in boreal forest aerosol particle number and volume concentration and their connection to particle formation, Tellus, 60, 495–508, doi:10.1111/j.1600-0889.2008.00366.x, 2008.

Ding, A. J., Fu, C. B., Yang, X. Q., Sun, J. N., Zheng, L. F., Xie, Y. N., Herrmann, E., Nie, W., Petäjä, T., Kerminen, V.-M., and Kulmala, M.: Ozone and fine particle in the western Yangtze River Delta: an overview of 1 yr data at the SORPES station, Atmos. Chem. Phys., 13, 5813–5830, doi:10.5194/acp-13-5813-2013, 2013a.

Ding, A. J., Fu, C. B., Yang, X. Q., Sun, J. N., Petäjä, T., Kerminen, V.-M., Wang, T., Xie, Y., Herrmann, E., Zheng, L. F., Nie, W., Liu, Q., Wei, X. L., and Kulmala, M.: Intense atmospheric pollution modifies weather: a case of mixed biomass burning with fossil fuel combustion pol-

lution in eastern China, Atmos. Chem. Phys., 13, 10545–10554, doi:10.5194/acp-13-10545-2013, 2013b.
Ding, A. J., Wang, T., and Fu, C. B.: Transport characteristics and origins of carbon monoxide and ozone in Hong Kong, South China, J. Geophys. Res., 118, 9475–9488, doi:10.1002/jgrd.50714, 2013c.
Draxler, R. R. and Hess, G. D.: An overview of the HYSPLIT 4 modeling system for trajectories dispersion and deposition, Aust. Meteorol. Mag., 47, 295–308, 1998.
Du, J. F., Cheng, T. T., Zhang, M., Chem, J. M., He, Q. S., Wang, X. M., Zhang, R. J., Tao, J., Huang, G. H., Li, X., and Zha, S. P.: Aerosol size spectra and particle formation events at urban Shanghai in Eastern China, Aerosol Air Qual. Res., 12, 1362–1372, doi:10.4209/aaqr.2011.12.0230, 2012.
Engler, C., Rose, D., Wehner, B., Wiedensohler, A., Brüggemann, E., Gnauk, T., Spindler, G., Tuch, T., and Birmili, W.: Size distributions of non-volatile particle residuals ($D_p < 800$ nm) at a rural site in Germany and relation to air mass origin, Atmos. Chem. Phys., 7, 5785–5802, doi:10.5194/acp-7-5785-2007, 2007.
Gao, J., Wang, T., Zhou, X. H., Wu, W. S., and Wang, W. X.: Measure of aerosol number size distributions in the Yangtze River delta in China: formation and growth of particles under polluted conditions, Atmos. Environ., 43, 829–836, doi:10.1016/j.atmosenv.2008.10.046, 2009.
Gettelman, A., Morrison, H., Terai, C. R., and Wood, R.: Microphysical process rates and global aerosol–cloud interactions, Atmos. Chem. Phys., 13, 9855–9867, doi:10.5194/acp-13-9855-2013, 2013.
Guo, H., Wang, D. W., Cheung, K., Ling, Z. H., Chan, C. K., and Yao, X. H.: Observation of aerosol size distribution and new particle formation at a mountain site in subtropical Hong Kong, Atmos. Chem. Phys., 12, 9923–9939, doi:10.5194/acp-12-9923-2012, 2012.
Hamed, A., Joutsensaari, J., Mikkonen, S., Sogacheva, L., Dal Maso, M., Kulmala, M., Cavalli, F., Fuzzi, S., Facchini, M. C., Decesari, S., Mircea, M., Lehtinen, K. E. J., and Laaksonen, A.: Nucleation and growth of new particles in Po Valley, Italy, Atmos. Chem. Phys., 7, 355–376, doi:10.5194/acp-7-355-2007, 2007.
Heal, M. R., Kumar, P., and Harrison, R. M.: Particles, air quality, policy and health, Chem. Soc. Rev., 41, 6606–6630, doi:10.1039/C2CS35076A, 2012.
Hennigan, C. J., Westervelt, D. M., Riipinen, I., Engelhart, G. J., Lee, T., Collett Jr., J. L., Pandis, S. N., Adams, P. J., and Robinson, A. L.: New particle formation and growth in biomass

ACPD
15, 12491–12537, 2015

burning plumes: an important source of cloud condensation nuclei, Geophys. Res. Lett., 39, L09805, doi:10.1029/2012gl050930, 2012.

Herrmann, E., Ding, A. J., Kerminen, V.-M., Petäjä, T., Yang, X. Q., Sun, J. N., Qi, X. M., Manninen, H., Hakala, J., Nieminen, T., Aalto, P. P., Kulmala, M., and Fu, C. B.: Aerosols and nucleation in eastern China: first insights from the new SORPES-NJU station, Atmos. Chem. Phys., 14, 2169–2183, doi:10.5194/acp-14-2169-2014, 2014.

Huang, X.-F., He, L.-Y., Xue, L., Sun, T.-L., Zeng, L.-W., Gong, Z.-H., Hu, M., and Zhu, T.: Highly time-resolved chemical characterization of atmospheric fine particles during 2010 Shanghai World Expo, Atmos. Chem. Phys., 12, 4897–4907, doi:10.5194/acp-12-4897-2012, 2012.

IPCC: Climate Change 2013: The Physical Science Basis, Contribution of Working Group I to the Fifth Assessment Report of the Intergovernmental Panel on Climate Change, edited by: Stocker, T. F., Qin, D., Plattner, G.-K., Tignor, M., Allen, S. K., Boschung, J., Nauels, A., Xia, Y., Bex, V., and Midgley, P. M., Cambridge University Press, Cambridge, UK, New York, NY, USA, 1535 pp., doi:10.1017/CBO9781107415324, 2013.

Jimenez, J. L., Canagaratna, M. R., Donahue, N. M., Prevot, A. S. H., Zhang, Q., Kroll, J. H., DeCarlo, P. F., Allan, J. D., Coe, H., Ng, N. L., Aiken, A. C., Docherty, K. S., Ulbrich, I. M., Grieshop, A. P., Robinson, A. L., Duplissy, J., Smith, J. D., Wilson, K. R., Lanz, V. A., Hueglin, C., Sun, Y. L., Tian, J., Laaksonen, A., Raatikainen, T., Rautiainen, J., Vaattovaara, P., Ehn, M., Kulmala, M., Tomlinson, J. M., Collins, D. R., Cubison, M. J., Dunlea, E. J., Huffman, J. A., Onasch, T. B., Alfarra, M. R., Williams, P. I., Bower, K., Kondo, Y., Schneider, J., Drewnick, F., Borrmann, S., Weimer, S., Demerjian, K., Salcedo, D., Cottrell, L., Griffin, R., Takami, A., Miyoshi, T., Hatakeyama, S., Shimono, A., Sun, J. Y., Zhang, Y. M., Dzepina, K., Kimmel, J. R., Sueper, D., Jayne, J. T., Herndon, S. C., Trimborn, A. M., Williams, L. R., Wood, E. C., Middlebrook, A. M., Kolb, C. E., Baltensperger, U., and Worsnop, D. R.: Evolution of organic aerosols in the atmosphere, Science, 326, 1525–1529, doi:10.1126/science.1180353, 2009.

Kerminen, V.-M., Lihavainen, H., Komppula, M., Viisanen, Y., and Kulmala, M.: Direct observational evidence linking atmospheric aerosol formation and cloud droplet activation, Geophys. Res. Lett., 32, L14803, doi:10.1029/2005gl023130, 2005.

Kerminen, V.-M., Paramonov, M., Anttila, T., Riipinen, I., Fountoukis, C., Korhonen, H., Asmi, E., Laakso, L., Lihavainen, H., Swietlicki, E., Svenningsson, B., Asmi, A., Pandis, S. N., Kulmala, M., and Petäjä, T.: Cloud condensation nuclei production associated with atmospheric

ACPD
15, 12491–12537, 2015

nucleation: a synthesis based on existing literature and new results, Atmos. Chem. Phys., 12, 12037–12059, doi:10.5194/acp-12-12037-2012, 2012.
Kivekäs, N., Sun, J., Zhan, M., Kerminen, V.-M., Hyvärinen, A., Komppula, M., Viisanen, Y., Hong, N., Zhang, Y., Kulmala, M., Zhang, X.-C., Deli-Geer, and Lihavainen, H.: Long term particle size distribution measurements at Mount Waliguan, a high-altitude site in inland China, Atmos. Chem. Phys., 9, 5461–5474, doi:10.5194/acp-9-5461-2009, 2009.
Komppula, M., Lihavainen, H., Hyvarinen, A. P., Kerminen, V.-M., Panwar, T. S., Sharma, V. P., and Visanen, Y.: Physical properties of aerosol particles at a Himalayan background site in India, J. Geophys. Res., 114, D12202, doi:10.1029/2008jd011007, 2009.
Kulmala, M. and Kerminen, V.-M.: On the formation and growth of atmospheric nanoparticles, Atmos. Res., 90, 132–150, doi:10.1016/j.atmosres.2008.01.005, 2008.
Kulmala, M., Vehkamaki, H., Petäjä, T., Dal Maso, M., Lauri, A., Kerminen, V.-M., Birmili, W., and McMurry, P. H.: Formation and growth rates of ultrafine atmospheric particles: a review of observations, J. Aerosol Sci., 35, 143–176, doi:10.1016/j.jaerosci.2003.10.003, 2004.
Kulmala, M., Petäjä, T., Nieminen, T., Sipilä, M., Manninen, H. E., Lehtipalo, K., Dal Maso, M., Aalto, P. P., Junninen, H., Paasonen, P., Riipinen, I., Lehtinen, K. E. J., Laaksonen, A., and Kerminen, V.-M.: Measurement of the nucleation of atmospheric aerosol particles, Nat. Protoc., 7, 1651–1667, doi:10.1038/nprot.2012.091, 2012.
Kulmala, M., Kontkanen, J., Junninen, H., Lehtipalo, K., Manninen, H. E., Nieminen, T., Petäjä, T., Sipila, M., Schobesberger, S., Rantala, P., Franchin, A., Jokinen, T., Jarvinen, E., Aijala, M., Kangasluoma, J., Hakala, J., Aalto, P. P., Paasonen, P., Mikkila, J., Vanhanen, J., Aalto, J., Hakola, H., Makkonen, U., Ruuskanen, T., Mauldin, R. L., Duplissy, J., Vehkamaki, H., Back, J., Kortelainen, A., Riipinen, I., Kurten, T., Johnston, M. V., Smith, J. N., Ehn, M., Mentel, T. F., Lehtinen, K. E. J., Laaksonen, A., Kerminen, V.-M., and Worsnop, D. R.: Direct observation of atmospheric aerosol nucleation, Science, 339, 943–946, doi:10.1126/science.1227385, 2013.
Kulmala, M., Petäjä, T., Ehn, M., Thornton, J., Sipilä, M., Worsnop, D. R., and Kerminen, V.-M.: Chemistry of atmospheric nucleation: on the recent advances on precursor characterization and atmospheric cluster composition in connection with atmospheric particle formation, Annu. Rev. Phys. Chem., 65, 21–37, doi:10.1146/annurev-physchem-040412-110014, 2014.
Laakso, L., Laakso, H., Aalto, P. P., Keronen, P., Petäjä, T., Nieminen, T., Pohja, T., Siivola, E., Kulmala, M., Kgabi, N., Molefe, M., Mabaso, D., Phalatse, D., Pienaar, K., and Kerminen, V.-M.: Basic characteristics of atmospheric particles, trace gases and meteorology in a rela-

ACPD
15, 12491–12537, 2015

tively clean Southern African Savannah environment, Atmos. Chem. Phys., 8, 4823–4839, doi:10.5194/acp-8-4823-2008, 2008.
Lebo, Z. J. and Feingold, G.: On the relationship between responses in cloud water and precipitation to changes in aerosol, Atmos. Chem. Phys., 14, 11817–11831, doi:10.5194/acp-14-11817-2014, 2014.
Li, L., Chen, C. H., Fu, J. S., Huang, C., Streets, D. G., Huang, H. Y., Zhang, G. F., Wang, Y. J., Jang, C. J., Wang, H. L., Chen, Y. R., and Fu, J. M.: Air quality and emissions in the Yangtze River Delta, China, Atmos. Chem. Phys., 11, 1621–1639, doi:10.5194/acp-11-1621-2011, 2011.
Li, X. H., Duan, L., Wang, S. X., Duan, J. C., Guo, X. M., Yi, H. H., Hu, J. N., Li, C., and Hao, J. M.: Emission characteristics of particulate matter from rural household biofuel combustion in China, Energy Fuels, 21, 845–851, doi:10.1021/ef060150g, 2007.
Liu, S., Hu, M., Wu, Z. J., Wehner, B., Wiedensohler, A., and Cheng, Y. F.: Aerosol number size distribution and new particle formation at a rural/coastal site in Pearl River Delta (PRD) of China, Atmos. Environ., 42, 6275–6283, doi:10.1016/j.atmosenv.2008.01.063, 2008.
Malm, W. C., Sisler, J. F., Huffman, D., Eldred, R. A., and Cahill, T. A.: Spatial and seasonal trends in particle concentration and optical extinction in the United-States, J. Geophys. Res., 99, 1347–1370, doi:10.1029/93jd02916, 1994.
McMurry, P. H., Fink, M., Sakurai, H., Stolzenburg, M. R., Mauldin, R. L., Smith, J., Eisele, F., Moore, K., Sjostedt, S., Tanner, D., Huey, L. G., Nowak, J. B., Edgerton, E., and Voisin, D.: A criterion for new particle formation in the sulfur-rich Atlanta atmosphere, J. Geophys. Res., 110, D22S02, doi:10.1029/2005jd005901, 2005.
Menon, S., Hansen, J., Nazarenko, L., and Luo, Y. F.: Climate effects of black carbon aerosols in China and India, Science, 297, 2250–2253, doi:10.1126/science.1075159, 2002.
Nie, W., Ding, A. J., Xie, Y. N., Xu, Z., Mao, H., Kerminen, V.-M., Zheng, L. F., Qi, X. M., Huang, X., Yang, X.-Q., Sun, J. N., Herrmann, E., Petäjä, T., Kulmala, M., and Fu, C. B.: Influence of biomass burning plumes on HONO chemistry in eastern China, Atmos. Chem. Phys., 15, 1147–1159, doi:10.5194/acp-15-1147-2015, 2015.
Nieminen, T., Asmi, A., Dal Maso, M., Aalto, P. P., Keronen, P., Petäjä, T., Kulmala, M., and Kerminen, V.-M.: Trends in atmospheric new-particle formation: 16 years of observations in a boreal-forest environment, Boreal Environ. Res., 19, 191–214, 2014.
Peng, J. F., Hu, M., Wang, Z. B., Huang, X. F., Kumar, P., Wu, Z. J., Guo, S., Yue, D. L., Shang, D. J., Zheng, Z., and He, L. Y.: Submicron aerosols at thirteen diversified sites in

ACPD
15, 12491–12537, 2015

China: size distribution, new particle formation and corresponding contribution to cloud condensation nuclei production, Atmos. Chem. Phys., 14, 10249–10265, doi:10.5194/acp-14-10249-2014, 2014.

Pope, C. A., Burnett, R. T., Thun, M. J., Calle, E. E., Krewski, D., Ito, K., and Thurston, G. D.: Lung cancer, cardiopulmonary mortality, and long term exposure to fine particulate air pollution, JAMA-J. Am. Med. Assoc., 287, 1132–1141, doi:10.1001/jama.287.9.1132, 2002.

Qian, Y., Leung, L. R., Ghan, S. J., and Giorgi, F.: Regional climate effects of aerosols over China: modeling and observation, Tellus B, 55, 914–934, doi:10.1046/j.1435-6935.2003.00070.x, 2003.

Raes, F., Van Dingenen, R., Vignati, E., Wilson, J., Putaud, J.-P., Seinfeld, J. H., and Adams, P.: Formation and cycling of aerosols in the global troposphere, Atmos. Environ., 34, 4215–4240, doi:10.1016/S1352-2310(00)00239-9, 2000.

Rao, S., Chirkov, V., Dentener, F., Van Dingenen, R., Pachauri, S., Purohit, P., Amann, M., Heyes, C., Kinney, P., Kolp, P., Klimont, Z., Riahi, K., and Schoepp, W.: Environmental modeling and methods for estimation of the global health impacts of air pollution, Environ. Model. Assess., 17, 613–622, doi:10.1007/s10666-012-9317-3, 2012.

Reid, J. S., Koppmann, R., Eck, T. F., and Eleuterio, D. P.: A review of biomass burning emissions part II: intensive physical properties of biomass burning particles, Atmos. Chem. Phys., 5, 799–825, doi:10.5194/acp-5-799-2005, 2005.

Shen, X. J., Sun, J. Y., Zhang, Y. M., Wehner, B., Nowak, A., Tuch, T., Zhang, X. C., Wang, T. T., Zhou, H. G., Zhang, X. L., Dong, F., Birmili, W., and Wiedensohler, A.: First long-term study of particle number size distributions and new particle formation events of regional aerosol in the North China Plain, Atmos. Chem. Phys., 11, 1565–1580, doi:10.5194/acp-11-1565-2011, 2011.

Sihto, S.-L., Mikkilä, J., Vanhanen, J., Ehn, M., Liao, L., Lehtipalo, K., Aalto, P. P., Duplissy, J., Petäjä, T., Kerminen, V.-M., Boy, M., and Kulmala, M.: Seasonal variation of CCN concentrations and aerosol activation properties in boreal forest, Atmos. Chem. Phys., 11, 13269–13285, doi:10.5194/acp-11-13269-2011, 2011.

Stanier, C. O., Khlysyov, A. Y., and Pandis, S. N.: Ambient aerosol size distributions and number concentrations measured during the Pittsburgh Air Quality Study (PAQS), Atmos. Environ., 38, 3275–3284, doi:10.1016/j.atmosenv.2004.03.020, 2004.

Tie, X. X. and Cao, J. J.: Aerosol pollution in China: present and future impact on environment, Particuology, 7, 426–431, doi:10.1016/j.partic.2009.09.003, 2009.

ACPD
15, 12491–12537, 2015

CC BY

Vakkari, V., Beukes, J. P., Laakso, H., Mabaso, D., Pienaar, J. J., Kulmala, M., and Laakso, L.: Long-term observations of aerosol size distributions in semi-clean and polluted savannah in South Africa, Atmos. Chem. Phys., 13, 1751–1770, doi:10.5194/acp-13-1751-2013, 2013.

Vakkari, V., Kerminen, V.-M., Beukes, J. P., Titta, P., van Zyl, P. G., Josipovic, M., Venter, A. D., Laars, K., Worsnop, D. R., Kulmala, M., and Laakso, L.: Rapid changes in biomass burning aerosols by atmospheric oxidation, Geophys. Res. Lett., 41, 2644–2651, doi:10.1002/2014gl059396, 2014.

Wang, H. L., Zhu, B., Shen, L. J., An, J. L., Yin, Y., and Kang, H. Q.: Number size distribution of aerosols at Mt. Huang and Nanjing in the Yangtze River Delta, China: effects of air masses and characteristics of new particle formation, Atmos. Res., 150, 42–56, doi:10.1016/j.atmosres.2014.07.020, 2014.

Wang, Y. G., Hopke, P. K., Chalupa, D. C., and Utell, M. J.: Long-term study of urban ultrafine particles and other pollutants, Atmos. Environ., 45, 7672–7680, doi:10.1016/j.atmosenv.2010.08.022, 2011.

Wehner, B., Birmili, W., Ditas, F., Wu, Z., Hu, M., Liu, X., Mao, J., Sugimoto, N., and Wiedensohler, A.: Relationships between submicrometer particulate air pollution and air mass history in Beijing, China, 2004–2006, Atmos. Chem. Phys., 8, 6155–6168, doi:10.5194/acp-8-6155-2008, 2008.

Wiedensohler, A., Cheng, Y. F., Nowak, A., Wehner, B., Achtert, P., Berghof, M., Birmili, W., Wu, Z. J., Hu, M., Zhu, T., Takegawa, N., Kita, K., Kondo, Y., Lou, S. R., Hofzumahaus, A., Holland, F., Wahner, A., Gunthe, S. S., Rose, D., Su, H., and Pöschl, U.: Rapid aerosol particle growth and increase of cloud condensation nucleus activity by secondary aerosol formation and condensation: a case study for regional air pollution in northeastern China, J. Geophys. Res., 114, D00G08, doi:10.1029/2008jd010884, 2009.

Wiedensohler, A., Birmili, W., Nowak, A., Sonntag, A., Weinhold, K., Merkel, M., Wehner, B., Tuch, T., Pfeifer, S., Fiebig, M., Fjäraa, A. M., Asmi, E., Sellegri, K., Depuy, R., Venzac, H., Villani, P., Laj, P., Aalto, P., Ogren, J. A., Swietlicki, E., Williams, P., Roldin, P., Quincey, P., Hüglin, C., Fierz-Schmidhauser, R., Gysel, M., Weingartner, E., Riccobono, F., Santos, S., Grüning, C., Faloon, K., Beddows, D., Harrison, R., Monahan, C., Jennings, S. G., O'Dowd, C. D., Marinoni, A., Horn, H.-G., Keck, L., Jiang, J., Scheckman, J., McMurry, P. H., Deng, Z., Zhao, C. S., Moerman, M., Henzing, B., de Leeuw, G., Löschau, G., and Bastian, S.: Mobility particle size spectrometers: harmonization of technical standards and data

ACPD
15, 12491–12537, 2015

structure to facilitate high quality long-term observations of atmospheric particle number size distributions, Atmos. Meas. Tech., 5, 657–685, doi:10.5194/amt-5-657-2012, 2012.

Woo, K. S., Chen, D. R., Pui, D. Y. H., and McMurry, P. H.: Measurement of Atlanta aerosol size distributions: observations of ultrafine particle events, Aerosol Sci. Tech., 34, 75–87, doi:10.1080/027868201300082049, 2001.

Wu, Z. J., Hu, M., Liu, S., Wehner, B., Bauer, S., Ssling, A. M., Wiedensohler, A., Petäjä, T., Dal Maso, M., and Kulmala, M.: New particle formation in Beijing, China: statistical analysis of a 1 year data set, J. Geophys. Res., 112, D09209, doi:10.1029/2006jd007406, 2007.

Wu, Z. J., Hu, M., Lin, P., Liu, S., Wehner, B., and Wiedensohler, A.: Particle number size distribution in the urban atmosphere of Beijing, China, Atmos. Environ., 42, 7967–7980, doi:10.1016/j.atmosenv.2008.06.022, 2008.

Yli-Juuti, T., Riipinen, I., Aalto, P. P., Nieminen, T., Ugent, W. M., Janssens, I. A., Claeys, M., Salma, I., Ocskay, R., Hoffer, A., Imre, K., and Kulmala, M.: Characteristics of new particle formation events and cluster ions at K-Puszta, Hungry, Boreal Environ. Res., 14, 683–698, 2009.

Zhang, Q., Jimenez, J. L., Canagaratna, M. R., Allan, J. D., Coe, H., Ulbrich, I., Alfarra, M. R., Takami, A., Middlebrook, A. M., Sun, Y. L., Dzepina, K., Dunlea, E., Docherty, K., DeCarlo, P. F., Salcedo, D., Onasch, T., Jayne, J. T., Miyoshi, T., Shimono, A., Hatakeyama, S., Takegawa, N., Kondo, Y., Schneider, J., Drewnick, F., Borrmann, S., Weimer, S., Demerjian, K., Williams, P., Bower, K., Bahreini, R., Cottrell, L., Griffin, R. J., Rautiainen, J., Sun, J. Y., Zhang, Y. M., and Worsnop, D. R.: Ubiquity and dominance of oxygenated species in organic aerosols in anthropogenically-influenced Northern Hemisphere multitudes, Geophys. Res. Lett., 34, L13801, doi:10.1029/2007GL029979, 2007.

ACPD
15, 12491–12537, 2015

Table 1. Overall statistics for the number concentrations and relevant parameters calculated based on DMPS measurement at the SORPES site during December 2011–November 2013.

	Annual	Spring	Summer	Autumn	Winter
Total particles (cm^{-3})	19 200[a] ± 9200[b]	20 600 ± 9000	18 000 ± 10 800	18 000 ± 7600	19 900 ± 9300
Nucleation mode (cm^{-3})	5300 ± 5500	6200 ± 5900	4600 ± 5500	4800 ± 4900	5700 ± 5400
Aitken mode (cm^{-3})	8000 ± 4400	8500 ± 4000	8100 ± 5700	7600 ± 3900	7800 ± 3900
Accumulation mode (cm^{-3})	5800 ± 3200	5900 ± 2900	5300 ± 4200	5600 ± 2500	6500 ± 3000
$GMD_{6-800\,nm}$ (nm)	92 ± 25	89 ± 23	90 ± 26	92 ± 26	97 ± 26
CS ($10^{-2}\,s^{-1}$)	4.4 ± 2.5	4.6 ± 2.3	4.0 ± 3.3	4.1 ± 2.1	4.8 ± 2.3

[a]: Mean, [b]: SD, $GMD_{6-800\,nm}$: Geometric Mean Diameter of 6–800 nm particles, CS: Condensation sink.

ACPD
15, 12491–12537, 2015

CC BY

Table 2. Statistics of NPF events, J_6, $GR_{6–30\,nm}$ and CS at the SORPES station during the two-year measurement period.

		Spring	Summer	Autumn	Winter
Event Classification	Class I	52	44	64	10
	Class II	42	29	24	5
	Non-event	75	60	89	115
	Undefine/no data	15	51	5	51
J_6 ($cm^{-3}\,s^{-1}$)	Mean ± SD	3.6 ± 2.4	2.1 ± 1.4	2.1 ± 1.9	1.8 ± 1.6
$GR_{6–30\,nm}$ ($nm\,h^{-1}$)	Mean ± SD	10.0 ± 3.4	12.8 ± 4.4	8.9 ± 2.9	9.5 ± 3.3
CS ($10^{-2}\,s^{-1}$)	Mean ± SD	3.3 ± 1.0	3.2 ± 1.3	2.8 ± 0.9	3.3 ± 0.8

ACPD
15, 12491–12537, 2015

CC BY

Table 3. Correlation coefficients of J_6, $GR_{6-30\,nm}$ and CS with main meteorological parameters and air pollutants.

	Temp (°C)	RH (%)	Rad ($W\,m^{-2}$)	O_3 (ppbv)	$PM_{2.5}$ ($\mu g\,cm^{-3}$)	SO_2 (ppbv)	NO_x (ppbv)	CS ($10^{-2}\,s^{-1}$)
J_6 ($cm^{-3}\,s^{-1}$)	0.10	−0.31*	0.32*	0.17*	0.01	0.11	−0.01	0.06
$GR_{6-30\,nm}$ ($nm\,h^{-1}$)	0.36*	0.27*	0.27*	0.38*	0.07	0.06	−0.14	0.33*
CS ($10^{-2}\,s^{-1}$)	0.28*	0.02	0.15	0.40*	0.62*	0.51*	0.40*	–

*: The correlation coefficient passes the statistical significant test ($p < 0.05$).

ACPD
15, 12491–12537, 2015

CC BY

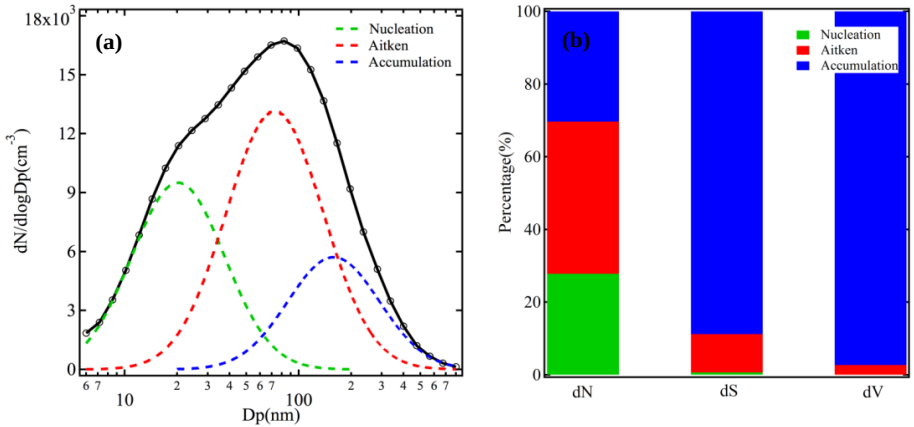

Figure 1. (a) Averaged number size distribution and lognormal fitting curves of three modes, and **(b)** averaged fraction of the particles number, surface and volume concentrations in the three modes measured at the SORPES site during December 2011–November 2013.

ACPD
15, 12491–12537, 2015

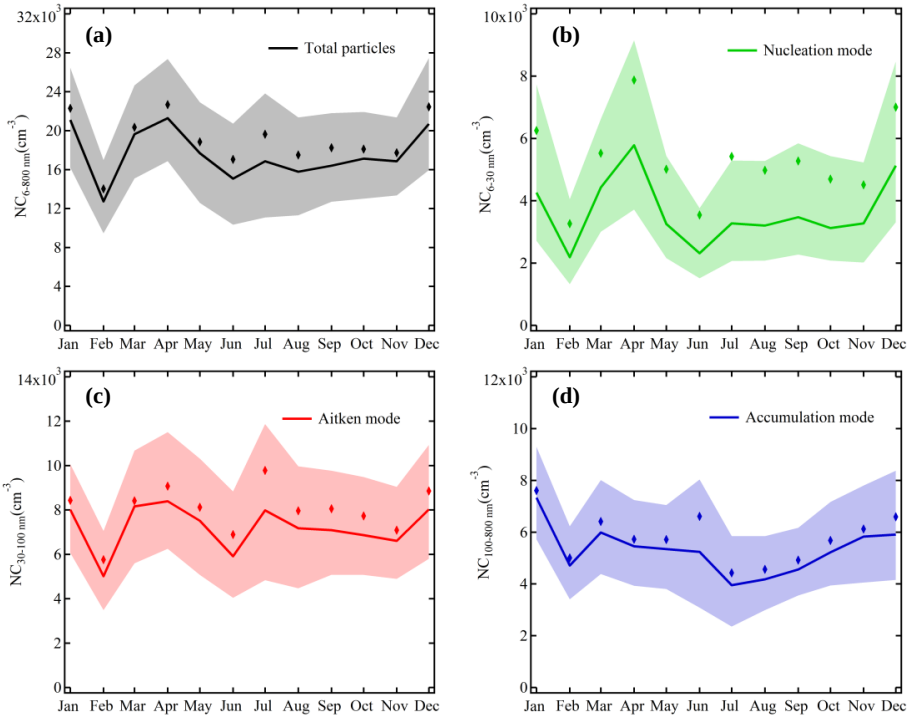

Figure 2. The averaged seasonal variations of **(a)** the total particle number concentration and number concentrations in the **(b)** nucleation, **(c)** Aitken and **(d)** accumulation mode. Note: Bold solid lines are the monthly median and shaded area represents the 25th or 75th percentiles. The diamond markers represent the monthly average.

ACPD
15, 12491–12537, 2015

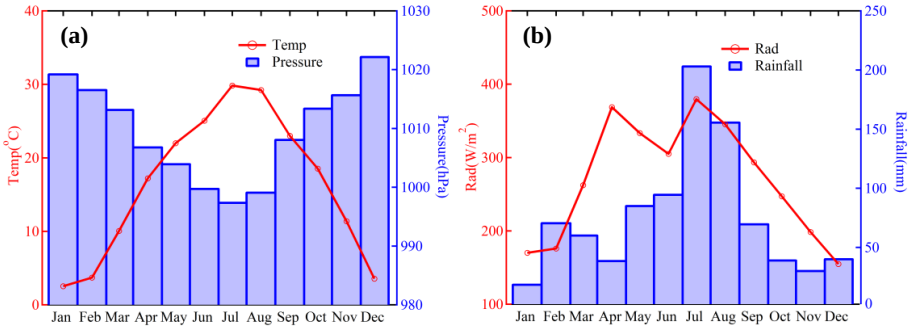

Figure 3. Averaged seasonal variations of **(a)** temperature and pressure, **(b)** radiation and rainfall during the entire measurement period.

ACPD
15, 12491–12537, 2015

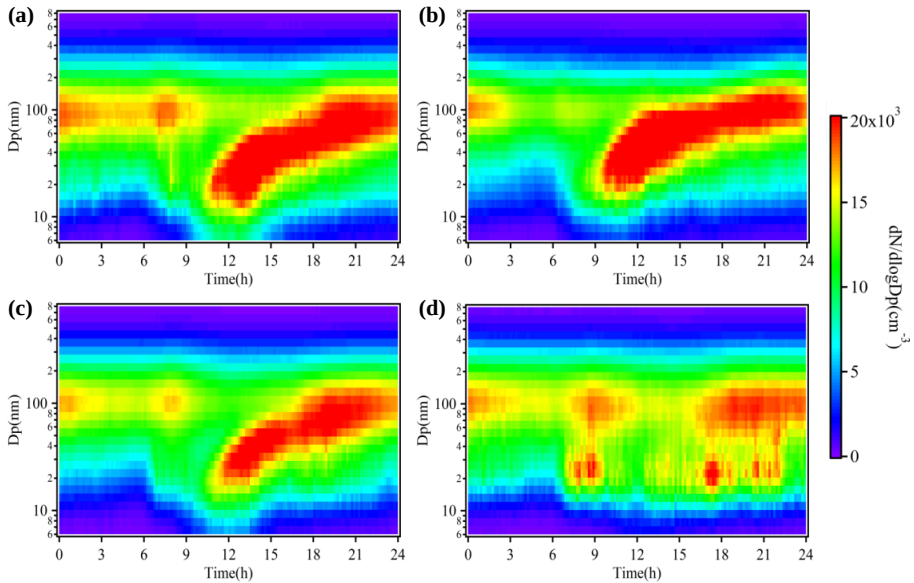

Figure 4. Averaged diurnal cycles of particle number size distributions for **(a)** spring, **(b)** summer, **(c)** autumn and **(d)** winter at the SORPES station during the 2-year measurement period.

ACPD
15, 12491–12537, 2015

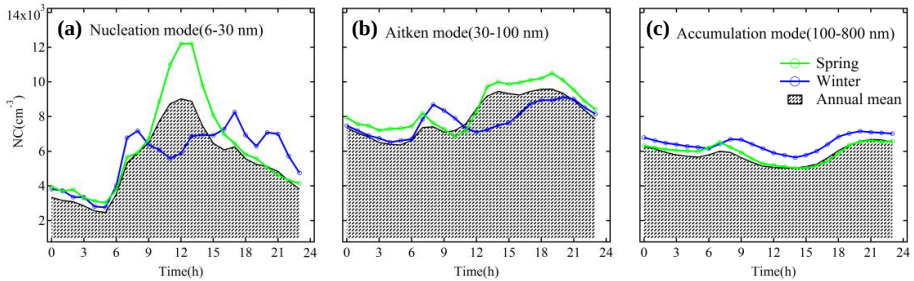

Figure 5. Averaged diurnal variations of particle number concentrations in **(a)** Nucleation mode, **(b)** Aitken mode, **(c)** accumulation mode in spring, winter and entire period during the two-year measurement period.

ACPD
15, 12491–12537, 2015

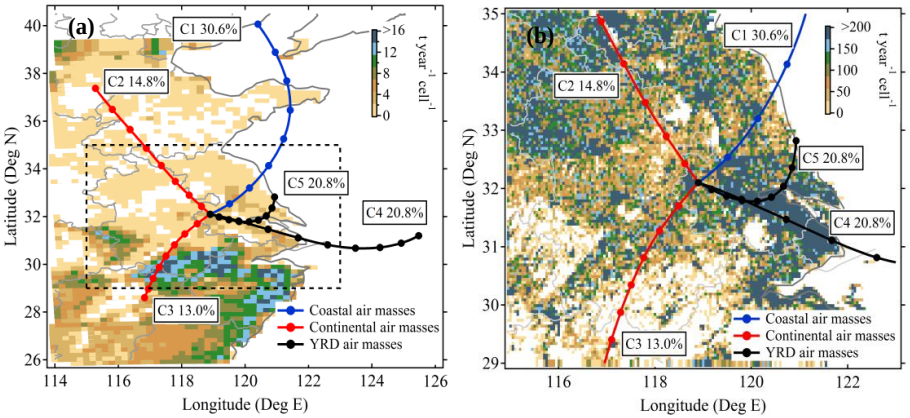

Figure 6. Mean air mass backward trajectories of five clusters showing on map of **(a)** biogenic volatile organic compounds (VOCs) in East China and **(b)** anthropogenic VOCs in the YRD. Note: Points of trajectories represent the six-hourly location. The percentages of each cluster are tabulated in the map. The biogenic VOCs data were calculated by MEGAN (the Model of Emissions of Gases and Aerosol from Nature) and the anthropogenic VOCs data were accessed from MEIC (Multi-resolution Emission Inventory for China) database (http://www.meicmodel.org/).

ACPD
15, 12491–12537, 2015

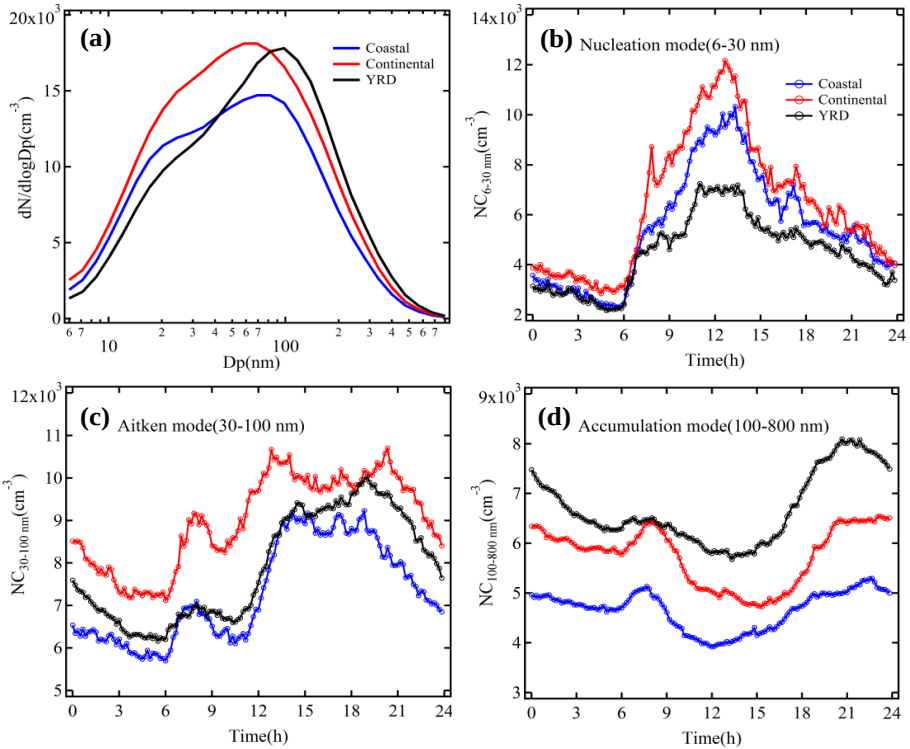

Figure 7. (a) Particles number size distributions of three air mass types; Diurnal variations of particle number concentration of three types of air masses in **(b)** nucleation, **(c)** Aitken and **(d)** accumulation mode.

ACPD
15, 12491–12537, 2015

CC BY

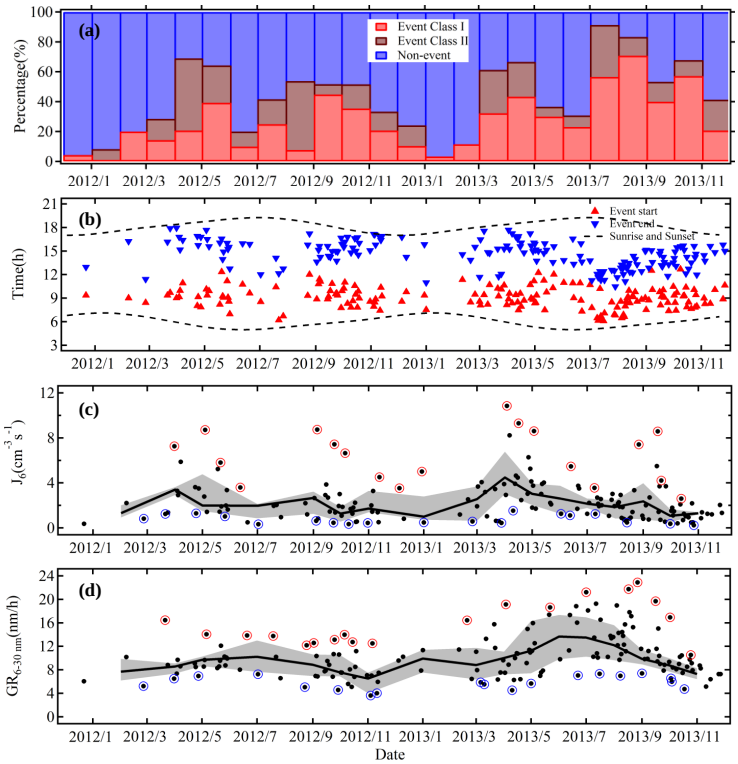

Figure 8. Monthly time series of **(a)** the fraction of Class I, Class II NPF events and non-event days, **(b)** start time and end time of Class I event days, **(c)** and **(d)** J_6 and growth rate during Class I event days. Note: Dashed lines in **(b)** represent the sunrise and sunset time. Bold solid lines in **(c)** and **(d)** are the median values and shaded area represents the 25th or 75th percentiles. Red circles and blue circles in **(c)** and **(d)** are the days that selected for further investigation in Sect. 3.2.3.

ACPD
15, 12491–12537, 2015

CC BY

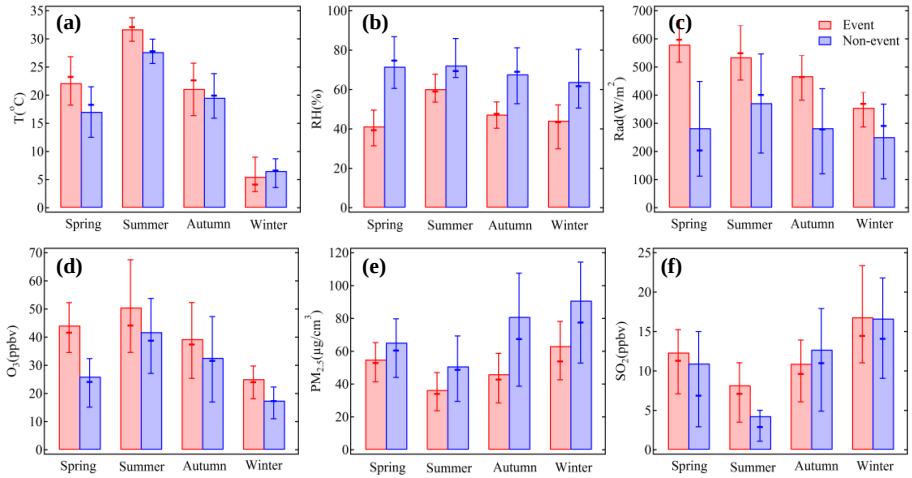

Figure 9. (a–c) meteorological variables and **(d–f)** gaseous pollutants during event (red) and non-event (blue) days in different seasons. Note: Bars are the mean value. The bold stick and whiskers are median values and 25th or 75th percentiles.

ACPD
15, 12491–12537, 2015

CC BY

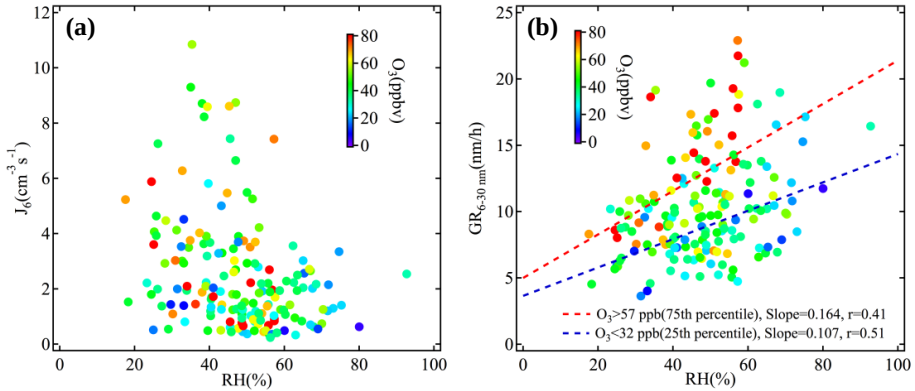

Figure 10. Scatter plot **(a)** between J_6 and RH and **(b)** between $GR_{6–30\,nm}$ and RH, color-coded with the O_3 concentration. Note: Linear fits for the data when the O_3 concentration is higher than 57 ppbv (the 75th percentile) or lower than 32 ppbv (the 25th percentile) are shown in **(b)**, respectively.

ACPD
15, 12491–12537, 2015

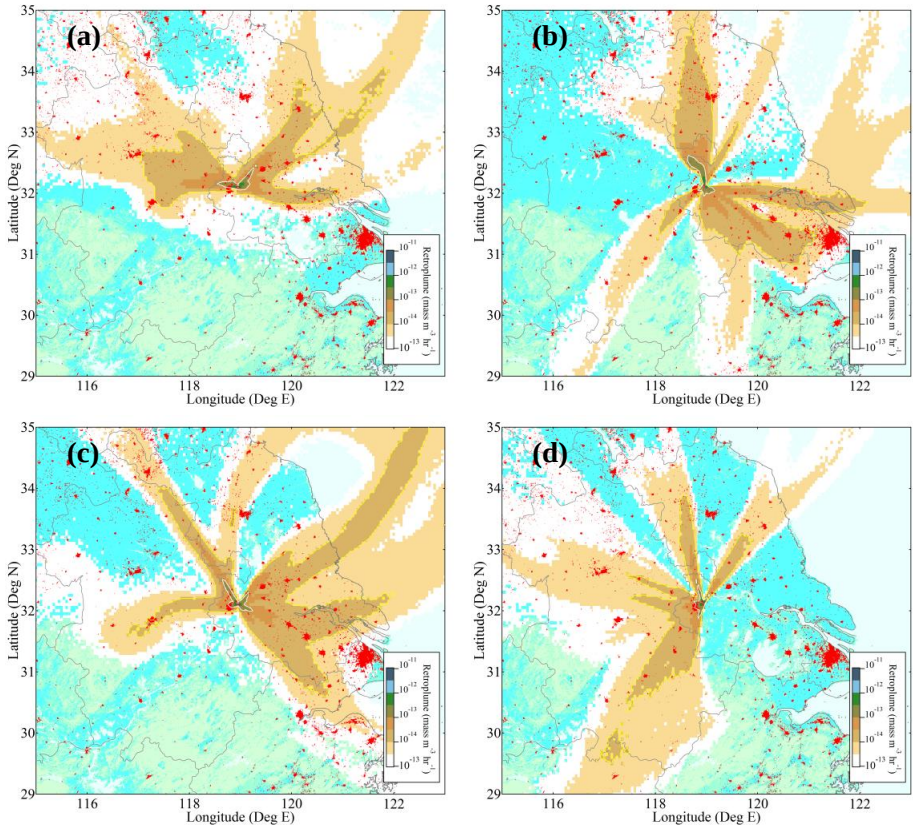

Figure 11. The averaged retroplumes (i.e. 100 m footprint) of the selected events: **(a)** high J_6, **(b)** low J_6, **(c)** high GR, **(d)** low GR days. Note: Red area in the maps shows the location and size of city.

ACPD
15, 12491–12537, 2015

CC BY

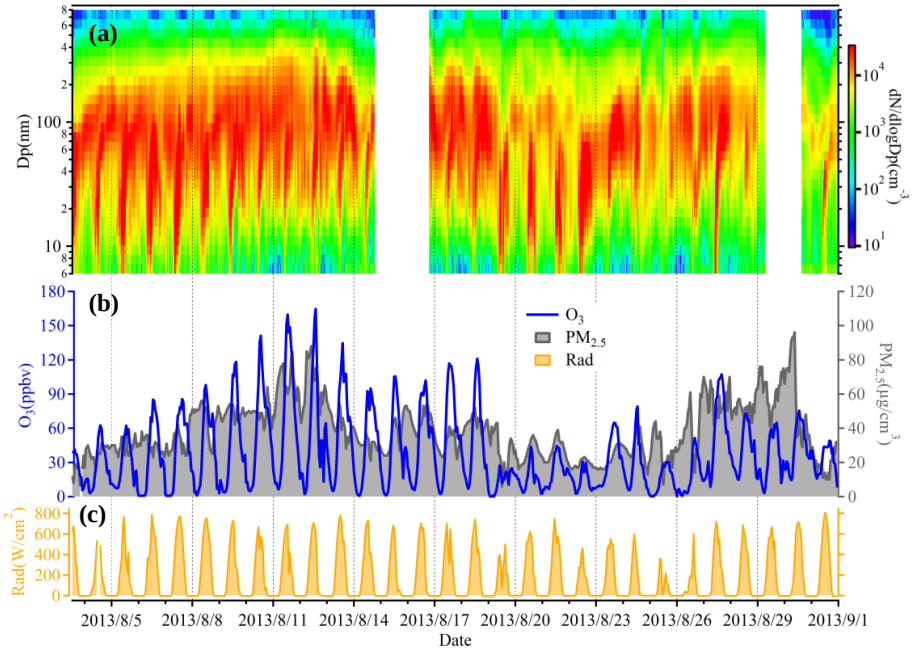

Figure 12. Time series of **(a)** particles number size distribution **(b)** O_3 and $PM_{2.5}$ concentrations and **(c)** intensity of radiation measured at SORPES site in August 2013.

ACPD
15, 12491–12537, 2015

CC BY

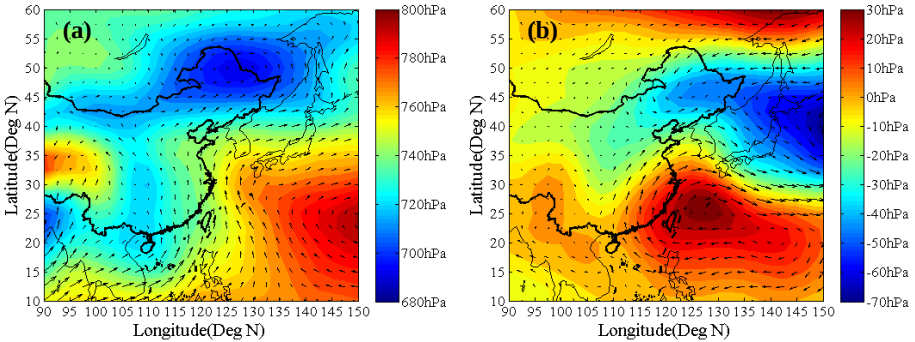

Figure 13. (a) Average geopotential height and wind vector at the 925 hPa level during August 2013. **(b)** Differences in geopotential height and wind vector between August 2013 and August 2012 at the 925 hPa level.

ACPD
15, 12491–12537, 2015

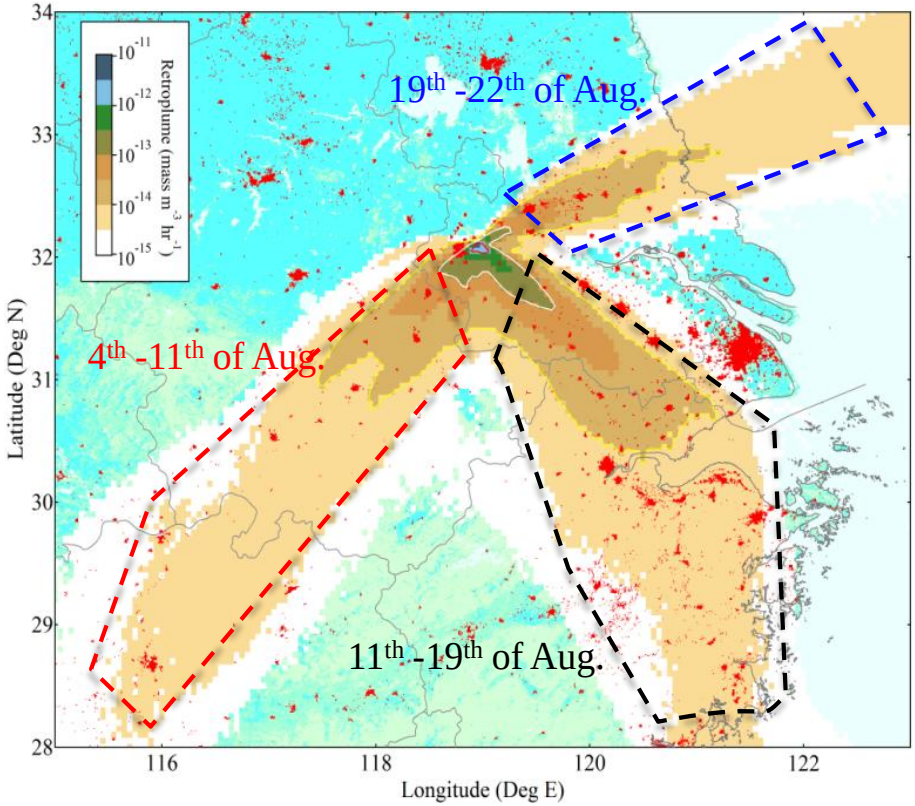

Figure 14. Retroplumes from 4 to 22 August 2013 identified with three main periods. Note: Red points denote the urban area.

ACPD
15, 12491–12537, 2015

CC BY

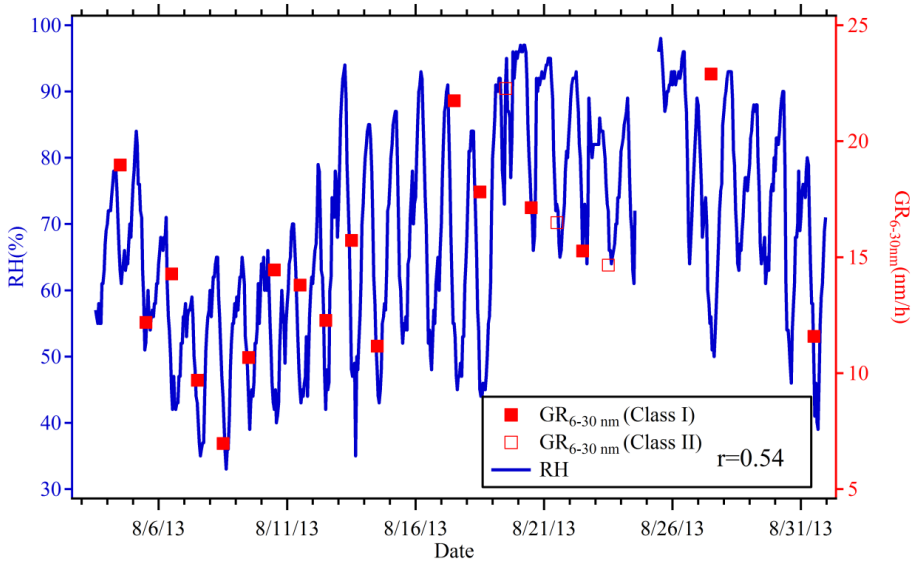

Figure 15. Time series of RH and the $GR_{6-30\,nm}$ of NPF days (Class I and Class II) in August 2013.

ACPD
15, 12491–12537, 2015

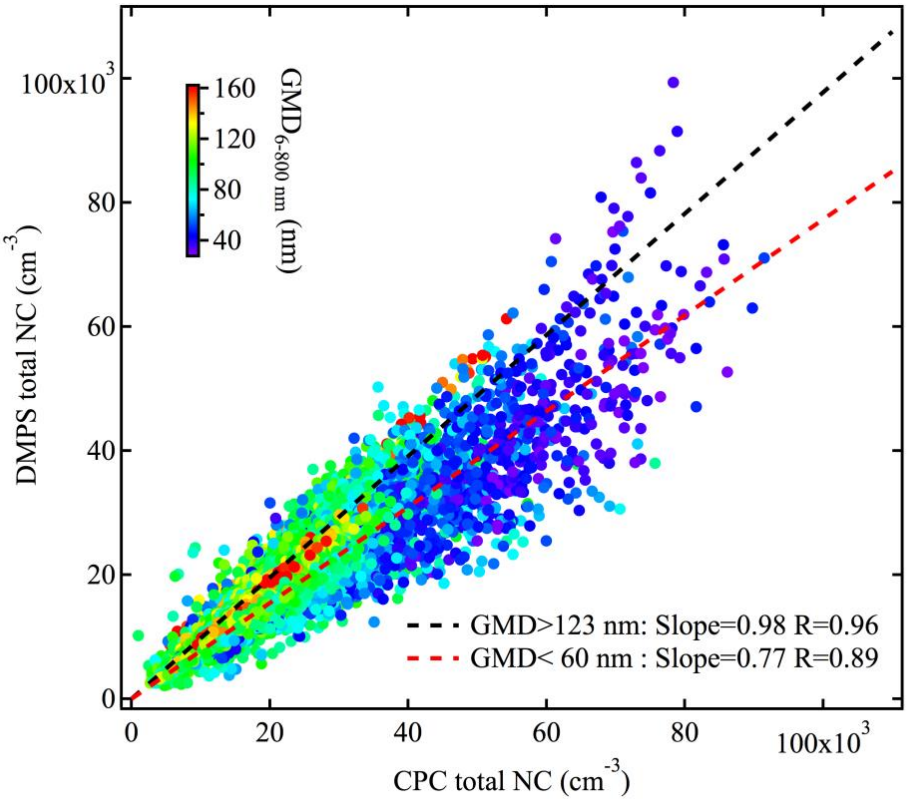

Figure A1. The scatter plot of N_{DMPS} vs. N_{CPC} color-coded with the geometric mean diameter of the particle number size distribution ($GMD_{6–800\,nm}$). Note: Linear fits for the data when the $GMD_{6–800\,nm}$ is higher than 123 nm (90th percentiles of the $GMD_{6–800\,nm}$ distribution) or lower than 60 nm (10th percentiles of the $GMD_{6–800\,nm}$ distribution) are shown in the figure.

ACPD
15, 12491–12537, 2015